

Hydroacoustic observation of Antarctic ice disintegration events in the Indian Ocean

B. Li (1) and A. N. Gavrilov (1)

(1) Centre for Marine Science & Technology, Curtin University of Technology, Perth, Australia

ABSTRACT

Rifting and breaking of ice shelves and icebergs in Antarctica produce intense pulse-like acoustic noise in the surrounding ocean, which can be detected thousands of kilometres away at the hydroacoustic receive stations deployed in the Indian Ocean as part of the International Monitoring System (IMS) of the Comprehensive Nuclear-Test-Ban Treaty (CTBT). A number of the most intense signals from Antarctic ice events observed at two IMS stations were selected to analyse their individual spectral characteristics and correlation and to verify the acoustic propagation model. The location of ice events derived from the back-azimuth estimates for signal arrivals at two stations was used to numerically predict the signal travel times using the seasonal temperature and salinity field from the World Ocean Atlas, and to compare the modelled and observed travel time differences. In most cases, the discrepancy in the even location derived from back-azimuth estimates and that derived from the travel time difference did not exceed 50 km, which justified the accurate location of events and verified the acoustic propagation model. Effects of normal mode coupling and transmission loss were also investigated through numerical modelling for different acoustic paths from Antarctica and compared with those observed experimentally.

INTRODUCTION

Different processes related to ice disintegration and motion on the Antarctic ice shelf generate acoustic noise of diverse temporal and spectral characteristics. Ice-generated noise is one of the major contributors to ocean ambient noise in the southern high-latitude ocean region and even in the temperate ocean thousands of kilometres away. Island-based seismic stations of the Polynesian Seismic Network in French Polynesia recorded the so-called T-phase signals, i.e. underwater acoustic waves transformed into ground waves over the coastal shelf, with a 4 to 7 Hz fundamental frequency and multiple overtones. These signals called harmonic tremors were associated with an iceberg drifting in the Ross Sea and generating acoustic signals presumably due to resonant vibrations or standing waves in either the solid ice plate of the iceberg or a water-filled cavity in the ice mass [Talandier et al 2002]. The oscillations were believed to be excited by the iceberg scraping against the seafloor. Chapp et al. [2004] observed two distinct types of low-frequency tremors received at the hydrophone stations in the Indian Ocean. The first, most frequently observed type is a long-lasting variable harmonic tremor of which the spectrogram reveals distinct harmonic lines varying slowly with time. Another type is the so-called cusped pulse tremor that has a pulsed waveform with curved harmonic bands in the spectrograms. Chapp et al. associated these two signal types with drifting icebergs and glacial processes along the Wilkes Land coast in Eastern Antarctica. They also hypothesised that the harmonic character of both tremor types could be explained by resonant vibrations in the ice plate of either icebergs or glaciers. Hanson and Bowman [2006] detected thousands of various hydroacoustic signals arrived to the IMS stations in the Indian Ocean from the Antarctic shelf. They did not distinguish signal types by their temporal and spectral characteristics and referred all of those signals to as ice events, hypothesizing that the most likely sources of such signals would be thermal fracturing and ridging of sea ice. An analysis of 8-month acoustic recordings made at the HA01 IMS station off Cape Leeuwin in Western Australia in 2003 has revealed a specific type of short, pulse-like signals that frequently arrive from

Antarctica and undergo strong negative frequency dispersion observed in their spectrograms as the main distinguishing feature [Gavrilov and Vazques, 2005]. Numerical modelling of the sound propagation from the Antarctic coast to the HA01 station has shown that the frequency dispersion is a result of sound propagation in the near-surface ocean acoustic waveguide in the polar environment south of the Antarctic Convergence and the signals are produced by short pulse-like physical processes on the Antarctic shelf, which are most likely ice rifting, breaking and collision events. Although the actual origin of such signals is not yet fully established, we will be referring to them in this paper as ice signals or ice events, because no other processes can currently be suggested as possible sources of pulse-like noise generated on the Antarctic shelf.

Access to the data from the HA08 IMS station installed off the Chagos Archipelago in the centre of the Indian Ocean substantially enhance the capability of acoustic detection and location of ice-related events on the Antarctic shelf. The station consists of two triads, i.e. three-hydrophone triangular horizontal arrays, of which the southern one (HA08S) is deployed 30 km south of the Diego Garcia US naval base in Chagos. The layout of the HA08 triads is similar to that of the HA01 station. The hydrophones are suspended via moorings near the axis of the SOFAR (Sound Fixing and Ranging) channel. Sea noise is sampled at 250 Hz with a dynamic range of 120 dB. The frequency band of the acoustic receiving system is from about 1 Hz to 100 Hz. The coverage area of the Antarctic coast by the H08S station is approximately from 10°E to 130°E. The back azimuth from H08S to the observable Antarctic coastline varies from -162° to 158°. The distance from the H08S station to the Antarctic shelf ranges from 6,000 km to 7,400 km, which is considerably longer than that from the HA01 station. The data recorded at HA08S station in 2003 are publicly accessible on the website of the U. S. Army Space and Missile Defence Command (SMDC) Monitoring Research Program (http://www.rdss.info/index_ie.html).

In this work, the location of several most intense ice events detected at both HA01 and HA08S stations is determined via intersection of the back-azimuth estimates of signal arrivals at two remote stations. Errors of acoustic location are also estimated using signal characteristics, system parameters and some assumptions made with respect to the uncertainty of the system geometry due to variations in the environmental conditions. Based on the location of ice events derived from the back-azimuth estimates for signal arrivals at two stations, the signal travel times are numerically modelled and the predicted arrival time difference is compared to that experimentally observed at two stations. In the last section, effects of acoustic mode coupling and transmission loss are considered using results of numerical modelling and experimental observation.

SIGNAL DETECTION AND LOCATION

In the previous work [Gavrilov and Vazques, 2005], the HA01 acoustic data collected from January to August 2003 have been processed and hundreds of pulse-like signals from the Antarctic shelf have been detected. In order to pick out the signals at the HA08S station from the same event as those detected at HA01, the following procedure was implemented: 1) The location of an ice event on the Antarctic shelf was roughly estimated by projection of the back-azimuth bearing from the HA01 station onto the Antarctic coast. 2) Based on the travel time difference to HA01 and HA08S estimated through acoustic propagation modelling, we determined the time interval within which the signal arrival at HA08S could be expected and then searched for a signal with similar waveform and spectral characteristics arrived at HA08S within the predicted time window. The search window was selected long enough to allow for possible errors in the numerical prediction of the travel time difference.

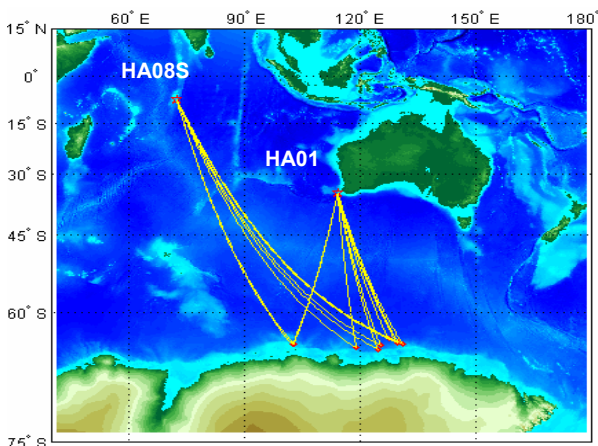


Figure 1. Back-azimuth bearing to nine Antarctic events observed at HA01 and HA08S. Red dots indicate the locations for events derived from the back-azimuth estimates.

Once the signal from the same Antarctic event is identified in the HA08S recordings, the event can be located at the intersection point of two great circles starting from the receive stations and bearing along the back-azimuth estimate for the signal arrival.

Assuming that the distance to the signal source is much larger than the triad dimension, a Plane Wave Fitting (PWF) method [Del Pezzo and Giudicepietro, 2002] can be applied to estimate the back-azimuth of signal arrivals at the receive stations. The arrival time difference t_{ij} for each pair of hydrophones in the triad was estimated through cross-correlation of the signal waveforms. The relation between the arrival time difference and the horizontal slowness \mathbf{p} of plane wave propagation can be expressed as the vector product

$$\mathbf{t} = \Delta\mathbf{x}\cdot\mathbf{p}, \tag{1}$$

where $\Delta\mathbf{x}$ denotes the relative position of hydrophones $\{x_i, y_i\}$ and \mathbf{p} is a two-element vector with horizontal components $\{p_x, p_y\}$. Because the number of linear equations in system (1) is larger than the number of unknown variables p_x and p_y , Eq.1 can be solved with respect to \mathbf{p} in the least-mean-squares sense, which can be expressed as follows:

$$\mathbf{p} = (\Delta\mathbf{x}^T\Delta\mathbf{x})^{-1}\Delta\mathbf{x}^T\mathbf{t}, \tag{2}$$

where T denotes the matrix transpose operation. The back-azimuth α and the group velocity v can then be calculated as $\alpha = \tan^{-1}(p_x/p_y)$ and $v = 1/|\mathbf{p}|$.

The Antarctic ice events detected at the HA01 station cannot always be observed at HA08S because of different propagation conditions, including propagation blockage by islands and shoals, along two different paths. For further analysis, we selected nine most intense ice signals detected at HA01 which were also observed at HA08S. The location of signal origin on the Antarctic shelf was derived from the back-azimuth estimates as shown in Figure 1. The detection time and the acoustically derived coordinates of these nine events are given in columns 1-5 of Table 1.

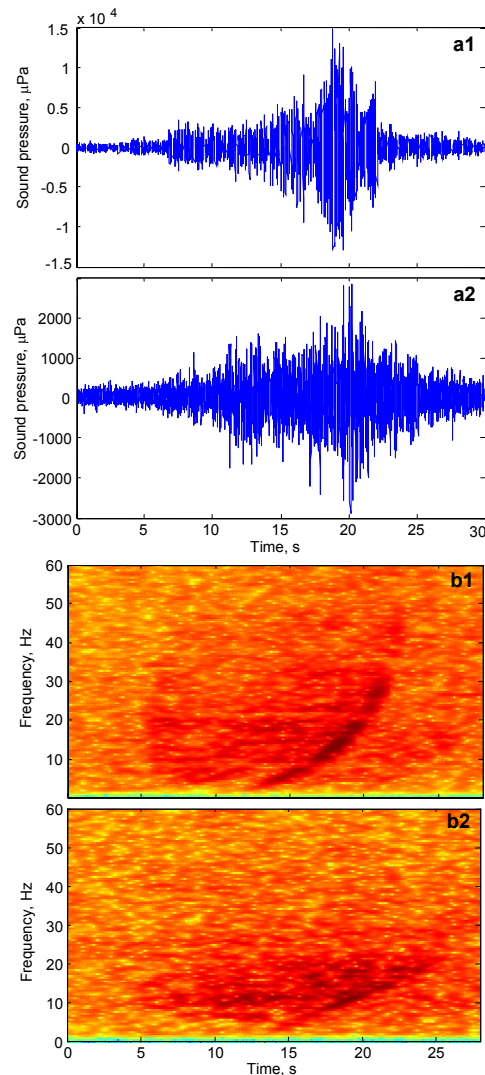


Figure 2. Typical waveforms (a) and spectrograms (b) of ice signals recorded at HA01 (1) and HA08S (2)

Table1. Arrival times of selected signals and coordinates of their origin located from the back-azimuth and verified via numerical modelling

Arrival date	Arrival at HA01 (h)	Arrival at H08S (h)	ΔT^a (h)	Back-azimuth location ^b	Modelled location ^c	ΔT Residual, ^d (s)	ΔL^e (km)
2003, 017	02.0306	02.7386	0.7080	[65.069°S, 118.936°E]	[66.864°S, 116.056°E]	118.7	239.13
2003, 055	04.8629	05.6627	0.7998	[64.289°S, 129.810°E]	[64.003°S, 130.415°E]	19.1	43.32
2003, 071	00.0091	00.8101	0.8010	[63.775°S, 127.307°E]	[63.585°S, 127.832°E]	-15.3	33.52
2003, 082	13.9080	14.5391	0.6311	[64.612°S, 102.388°E]	[64.672°S, 102.808°E]	-11.8	21.16
2003, 083	17.1758	17.9500	0.7742	[65.299°S, 124.554°E]	[65.029°S, 125.279°E]	-21.7	45.41
2003, 087	02.6669	03.4706	0.8037	[64.410°S, 129.491°E]	[64.220°S, 129.616°E]	-8.5	22.03
2003, 102	08.2570	08.8750	0.6180	[64.527°S, 102.694°E]	[64.467°S, 102.084°E]	17.6	30.07
2003, 133	22.1207	22.9292	0.8085	[64.551°S, 131.036°E]	[64.311°S, 131.546°E]	-15.8	36.33
2003, 158	01.7799	02.5542	0.7743	[64.764°S, 125.291°E]	[64.864°S, 124.976°E]	8.9	18.66

^a Signal arrival time difference observed at HA01 and HA08S (hours)

^b Location of events derived from intersection of the back-azimuths from two receive stations

^c Location of events that are consistent with the arrival time difference at two stations and closest to the location estimates by back-azimuth intersection

^d Difference between the observed arrival time difference at two stations and the travel time difference modelled for the location derived from back-azimuth estimates (seconds)

^e Distance between the back-azimuth location and the modelled curve satisfying the travel time difference at two stations

Figure 2 shows the waveform and spectrogram of one of the signals from the same ice event observed at both HA01 and HA08S stations. The waveforms of these two signals look similar, but the signal amplitude at HA08S is considerably lower than that at HA01. The frequency band of the ice signals received at HA01 typically ranges from several Hz to 20-30 Hz. In most cases, the signal consists of one prominent arrival pulse dispersed over frequency, which clearly seen in the spectrogram (panel b1 in Fig. 2). This pulse is believed to be mode 1 propagating with the least transmission loss, as demonstrated earlier by numerical modelling [Gavrilov and Vazques 2005]. A much smaller part of acoustic energy arrives earlier than mode 1, but it does not form a distinct pulse because of random-like dispersion over time and frequency. At HA08S, the frequency band of ice signals is generally narrower and limited to approximately 20 Hz. The spectrograms of ice signals at HA08S have a less definite modal appearance, although the pulse of mode 1 can be recognized in the spectrogram in the end of the signal arrival. Frequency dispersion of mode 1 at HA08 is noticeably stronger and the energy contribution from the noise-like precursor is relatively higher than that at HA01. Higher attenuation at higher frequencies and stronger frequency dispersion along the paths to HA08 are most likely a result of longer propagation in the polar environment south of the Antarctic Convergence (see Fig.1) where the transmission loss due to surface scattering by sea ice and waves is much higher than that in the temperate ocean, especially at higher frequencies, and strong frequency dispersion features acoustic propagation in the near-surface acoustic channel.

The accuracy of back-azimuth estimates via PWF is constrained by the errors of the differential travel time estimates \mathbf{t} which depend on the Signal-to-Noise Ratio (SNR), the signal bandwidth and duration. The covariance matrix of the slowness \mathbf{p} can be derived from Eq. 2, as follows [Menke, 1984]:

$$\text{cov}(\mathbf{p}) = [(\Delta\mathbf{x}^T \Delta\mathbf{x})^{-1} \Delta\mathbf{x}] \text{cov}(\mathbf{t}) [(\Delta\mathbf{x}^T \Delta\mathbf{x})^{-1} \Delta\mathbf{x}]^T, \quad (3)$$

If the components of the travel time difference \mathbf{t} are normally distributed, the x and y components of the slowness \mathbf{p} will also be normally distributed. The diagonal elements of $\text{cov}(\mathbf{t})$ are the variance of the differential travel time estimates t_{ij} measured through cross-correlation of the signals at two different receivers i and j . This variance can be estimated as [Julius and Allan, 1985]:

$$\sigma^2(t_{ij}) \approx \frac{0.865}{(\pi B)^2} \varepsilon \left[\hat{R}_{ij}(t_{ij}) \right], \quad (4)$$

where

$$\varepsilon \left[\hat{R}_{ij}(t_{ij}) \right] \approx \frac{1}{2BT} \left[2 + \text{SNR}_i^{-1} + \text{SNR}_j^{-1} + (\text{SNR}_i \times \text{SNR}_j)^{-1} \right]$$

is the mean square error of the correlation coefficient estimate for two signals $S_i(t)$ and $S_j(t)$, B is the frequency bandwidth, T is the signal length, SNR_i and SNR_j are the signal-to-noise ratio of signals $S_i(t)$ and $S_j(t)$ respectively. The SNR of the most signals selected for this analysis exceeds 10 dB, the bandwidth is about 20-30 Hz and the signal duration is approximately 10 seconds. Hence the STD of the time delay estimates should not exceed 1 millisecond, which is smaller than the 4-millisecond sampling interval of the IMS hydroacoustic recordings. The errors of the correlation maximum location due to quantization are uniformly distributed within the sampling interval Δt with the variance $\sigma^2(t) = \Delta t^2/12$. These errors are statistically independent for different pairs of receivers, so that the non-diagonal elements of the covariance matrix $\text{cov}(\mathbf{t})$ in Eq.3 are all zeros and the main diagonal elements are $\Delta t^2/12$. Once the covariance matrix of the slowness \mathbf{p} is determined from Eq.3, the standard deviation of the back-azimuth estimate can be found using an approximation for small variations. The back-azimuth variance can be expressed as:

$$\text{var}(\varphi) = \left\langle \left[\tan^{-1} \left(\frac{\hat{p}_x + \delta p_x}{\hat{p}_y + \delta p_y} \right) - \tan^{-1} \left(\frac{\hat{p}_x}{\hat{p}_y} \right) \right]^2 \right\rangle,$$

where \hat{p}_x and \hat{p}_y are the mean values of the slowness components derived from Eq.2, and δp_x and δp_y are statistical errors of the estimate. Then applying the formula for arctangent difference, expanding $\text{var}(\varphi)$ about \hat{p}_x and \hat{p}_y , and ignoring all terms of the order higher than $O(\delta p_{x,y})$, one can obtain:

$$\text{var}(\varphi) \approx \frac{\sigma^2(\delta p_x) \hat{p}_y^2 - \text{cov}(\delta p_x \delta p_y) \hat{p}_x \hat{p}_y + \sigma^2(\delta p_y) \hat{p}_x^2}{\hat{p}_x^4 + 2 \hat{p}_x^2 \hat{p}_y^2 + \hat{p}_y^4}, \quad (5)$$

where $\sigma^2(\delta p_{x,y})$ and $\text{cov}(\delta p_x \delta p_y)$ are the main diagonal and off-diagonal elements of the matrix $\text{cov}(\mathbf{p})$ respectively.

If the bearing estimates contain only quantization errors, then the standard deviation of bearing from both IMS stations should be less than 0.1° .

The bearing errors due to the horizontal motion of the hydrophones mounted on long vertical moorings can be much larger than the quantization error. In the absence of real data on the motion of individual receivers in the IMS stations, we made the following assumptions to estimate possible bearing errors due to deviation of the receivers' horizontal position. The horizontal deviation of the receivers in each particular station is likely to have a common component resulted from the general current field, which can be variable in time, but nearly uniform in the horizontal dimension within the array span of about 2 km. This common component can be as large as several tens of metres, but it does not influence the errors of bearing to remote sources. Smaller scale components different for different moorings are likely to be superimposed on the common deviation component because of small differences in the local current profiles and slightly different length of the moorings. We assume that these differential components of receivers' horizontal deviation are random, normally distributed, and statistically independent, i.e. incoherent. Based on such assumptions, the slowness covariance matrix can be estimated using Eq.3, in which the receivers' relative position Δx is taken to be the expected values, i.e. the bottom touchdown location of the moorings, and the horizontal deviation of the receivers is accounted for in the variance of the differential travel time. If the incoherent deviation of individual receivers is horizontally isotropic and has the standard deviation δx , then the elements of the covariance matrix $cov(\mathbf{t})$ in Eq.3 are:

$$t_{ij} = \begin{cases} 2\delta x^2 / c^2, & i = j \\ \delta x^2 / c^2, & |i - j| = 1 \\ -\delta x^2 / c^2, & |i - j| = 2 \end{cases} \quad (6)$$

where c is the wave phase velocity, which is approximately equal to the local sound speed.

Figure 3 shows the root-mean-square (RMS) bearing error estimated for the HA01 station using Eqs. 3, 5, and 6 for different back-azimuths within the full sector of $0-360^\circ$ and different standard deviations δx of the receivers' position.

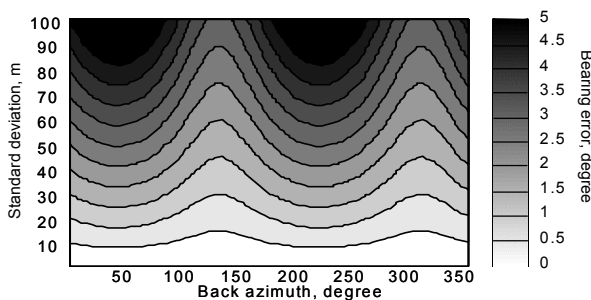


Figure 3. RMS bearing errors from HA01 as a function of the back-azimuth to the source and the standard deviation of the receivers' horizontal position.

As seen from Fig. 3, the uncertainty of receivers' position is much more critical for bearing errors than the errors of differential travel time estimates. In the further analysis, we assume that the incoherent horizontal deviation of the hydrophones is about 10 m RMS and, consequently, the RMS error of bearing is approximately 0.5° .

The back-azimuth estimates from two remote stations are statistically independent and also normally distributed if the above assumptions for small deviations are correct. In that

case, the source location estimates remain with certain probability within the ellipse of corresponding confidence level. The 90% confidence ellipses of four selected ice events located by signal bearing from HA01 and HA08S are shown in Figure 4.

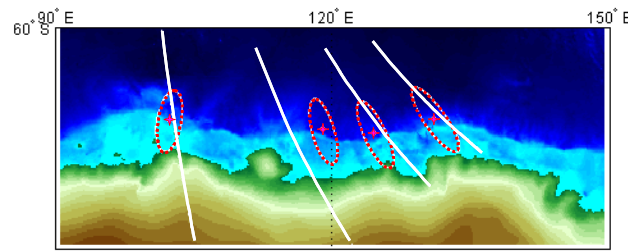


Figure 4. The 90% confidence ellipses of the location of four selected events detected at HA01 and HA08S. The white solid lines show the source locations that satisfy the travel time difference of signals measured at HA01 and HA08S.

OBSERVED AND MODELLED TRAVEL TIME DIFFERENCE

A numerical model of acoustic propagation from Antarctica to the Indian Ocean has been developed in the previous study based on the adiabatic mode approximation. The sound speed profiles along the paths from the Antarctic coast to HA01 and HA08S can be modelled using the gridded CTD data given for four seasons in the World Ocean Atlas 2001. The travel times of signals from ice events to the IMS stations can be numerically predicted for a known source location. However, the source location cannot be derived via inversion from the signal arrival times at to remote receivers. In a horizontally stratified ocean with no range dependence of the sound speed, the multiple source locations that satisfy the travel time difference constitute a hyperbola. In the real ocean environment, the solution of the inverse problem lies along more complicated lines of which the points can be found only approximately through numerical modelling of acoustic propagation in a gridded 3-D sound field and bathymetry [Chapp et al, 2004]. Nevertheless, a comparison of the observed and predicted travel time differences provides effective verification of the source location derived from back-azimuth measurements.

Because the ice signals were significantly dispersed, we estimated the signal arrival time by the arrival peak of mode 1 within a relatively narrow frequency band of the highest spectral level (~10–15 Hz). The accuracy of arrival time measurements in a narrow frequency band is about 0.5 s. The area for searching for the points that satisfy the arrival time differences measured at two stations was limited to a 5×5 degree grid around the location derived from back-azimuth intersection (column 5 in Table 1). Then the travel times from the grid nodes to the receive station were numerically predicted for the corresponding seasonal environmental conditions and the inverse solution curve was evaluated through spatial interpolation. For most of the selected events, the inverse solution curve crosses the 90% confidence ellipse of the event location (Figure 4), and the shortest distance from the back-azimuth location to the curve is less than 50 km (see the last column in Table 1). This means that the results of numerical prediction are consistent with the experimental observation and the back-azimuth location of events is in agreement with the signal arrival time measurements.

EFFECTS OF MODE COUPLING

Variable bathymetry and horizontal gradients in the sound speed field along the acoustic path cause coupling of acoustic

modes propagated in a range dependent ocean channel, which may lead to noticeable variations of the modal travel times and amplitudes [Gavrilov and Mikhalevsky, 2001 and 2006]. Any acoustic path from Antarctica to the IMS stations in the Indian Ocean is essentially range dependent, because it must cross the Antarctic continental slope, the Antarctic Convergence, and the continental slope near the receive station. Therefore, it is important to investigate possible effects of mode coupling on the modal travel times and amplitudes that may affect location of the ice events. Considering the range dependence of acoustic propagation conditions along the paths from Antarctica to be not very strong, an approximate solution for the complex amplitudes of coupled modes in a range dependent waveguide [Chiu et al., 1995; Gavrilov and Mikhalevsky, 2001] can be used to analyse the mode coupling effects. The top panel in Figure 5 shows the sound speed section along the path from 66°S, 119°E on the Antarctic shelf to the HA01 station in the summertime in the Southern Hemisphere. Both continental slopes at the beginning and end of the path are quite steep. The mid-ocean ridge is not high enough to influence sound propagation in the SOFAR channel. There is a sharp frontal zone at the Antarctic Convergence in the middle of the acoustic path, which is clearly seen in Figure 5. Variations of the amplitudes of modes 1 - 5 at 20 Hz along the path are shown in the lower panel of Figure 5 disregarding cylindrical spreading. The mode coupling effects are visible as rapid fluctuations of the modal amplitudes with the distance. Note that mode coupling affects the amplitudes of low-order modes only over the Antarctic continental slope and across the Antarctic Convergence. Mode coupling in the frontal zone is relatively weak, so that it does not influence much the amplitudes and travel times of modes at the receiver and therefore can be ignored in the model to speed up numerical calculations. In contrast to the frontal zone, the effect of the Antarctic continental slope can be strong depending on the bathymetry along this section. Unfortunately, the bathymetry samples on the Antarctic continental shelf are very sparse and therefore the ETOPO 2-minute gridded topography database for this seafloor region is generally not accurate. This means that the results of numerical prediction for acoustic propagation over the Antarctic shelf and slope may differ much from the real conditions.

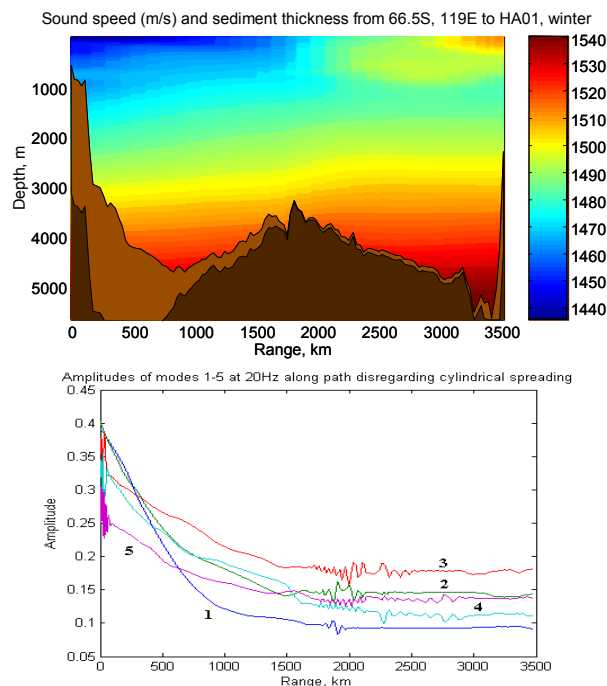


Figure 5. Top panel: Sound speed section along the selected path from the Antarctic shelf (66°S, 119°E) to the HA01 station. The light brown layer shows the total sediment thick-

ness. Bottom panel: Amplitudes of modes 1-5 at 20 Hz along the path disregarding cylindrical spreading.

As seen in Figure 5, mode 1 is least sensitive to sea depth variations on the Antarctic shelf, because this mode at frequencies above 15 Hz is trapped by the near-surface channel and its interaction with the seafloor is almost negligible. At lower frequencies and for higher modes, bathymetry features of the coastal shelf and continental slope may strongly affect the modal propagation characteristics including the group velocity and attenuation. Sea depth at the receiver is large enough for not affecting the low-order modes that carry most of the signal energy. Overall, the difference between the adiabatic and coupled-mode numerical prediction of the modal amplitudes and travel times is small enough to ignore the mode coupling effects, especially for mode 1 that dominates the higher mode at both HA01 and HA08 receive stations.

TRANSMISSION LOSS PREDICTION

The adiabatic-mode model was used to calculate the acoustic transmission loss and to trace the propagation blockage by islands and seabed ridges along different paths from the Antarctic coast to the HA01 and HA08S receive stations in the Indian Ocean. Two major factors influence the transmission loss of low frequency signals propagated from the Antarctic shelf. These factors are interaction with the seafloor over shallow water regions and sea surface scattering in the polar environment. To model these phenomena, it is critical to define appropriate boundary conditions, such as the structure and acoustic properties of the sediments and the spectral characteristics of surface waves and sea ice roughness. None of those characteristics has been sufficiently investigated in the sub-Antarctic seas. Therefore, in the model, we used parameters typical for the temperate ocean, except for the surface wave height which was assumed to be considerably larger (3 m to 5 m RMS) in the Southern Ocean than that in the temperate ocean, according to remote sensing observations from satellites. For the seafloor, we chose a one-layer sediment model overlaying a rigid basement. The thickness of the sediment layer was modelled varying with range according to the NGDC digital total sediment thickness database. The variations of transmission loss at 20-Hz and within the fre-

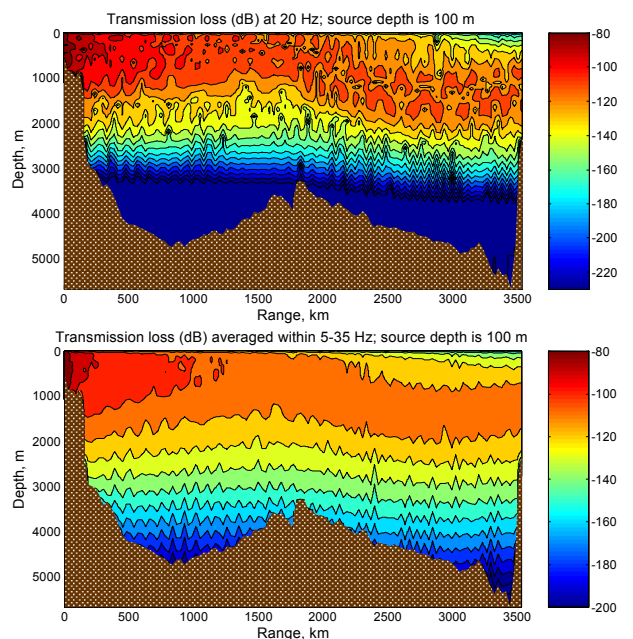


Figure 6. Top panel: Transmission loss at 20 Hz modelled along the path from 66°S, 119°E to HA01 for the source depth of 100 m. Bottom panel: Same as the top panel, but for the transmission loss averaged within 5 - 35 Hz.

quency band from 5 Hz to 35 Hz (average) modelled along the acoustic path from Antarctica to HA01 are shown in Figure 6 in the top and bottom panels respectively. These results were obtained for the sound speed field and bathymetry shown in Figure 5 and the source depth of 100 m.

Figure 6 clearly illustrates the difference between acoustic propagation south and north of the Antarctic Convergence. In the polar region of the Southern Ocean, the acoustic energy is canalised near the sea surface and affected by the surface roughness. At the Antarctic Convergence, the acoustic energy rapidly dives into the deep SOFAR acoustic channel and interacts very little with the sea surface and the seafloor.

The total transmission losses numerically predicted for mode 1 for various paths from the Antarctic coastline to the HA01 and HA08S stations are shown in Figure 7. For this modelling test, the signal frequency was chosen 20 Hz with the source depth of 40 m. Although the transmission loss undergoes noticeable short-scale variations due to different bathymetric features along the coast, general correlation with the length of the polar section of acoustic paths can be distinguished. For HA08S, the acoustic propagation from the Antarctic coast sector from approximately 64°E to 67°E is totally blocked by Heard and McDonald Islands and shoals around them. The wide blockage sector from about 74°E to 80°E corresponds to the inner part of the Amery Ice Shelf which is screened from HA01 by the Ingrid Christensen Coast.

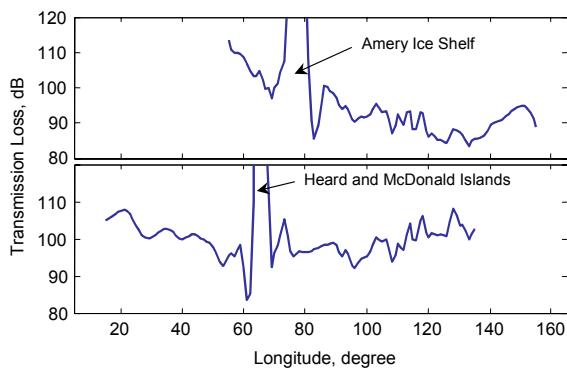


Figure 7. Total transmission loss of mode 1 from the observable sector of the Antarctic coast to the hydroacoustic stations HA01 (top) and HA08S (bottom)

CONCLUSION

The sources of several acoustic signals observed thousands of km away at two remote IMS hydroacoustic stations in the Indian Ocean were located on the Antarctic shelf using back-azimuth bearing from these two stations. Location errors were estimated based on the receive system parameters. The

location of events derived from the back-azimuth measurements is consistent with the signal arrival time difference at the stations and the results of numerical modelling of acoustic propagation. The error of location verified by the travel time difference does not exceed 50 km for most of the observed events. The signals from the same events received at the IMS stations have generally similar waveforms and spectrograms, but different amplitudes and frequency bands. Mode 1 dominates all other modes in the signals received at both stations. Numerical modelling has also shown that the mode coupling effects can be ignored almost everywhere along the acoustic propagation path from Antarctica, except for a relatively short initial section over the Antarctic continental shelf and slope. Mode 1 contributing most to the signal energy at the receivers is least sensitive to mode coupling and interaction with the seafloor. Acoustic observation of the Eastern Antarctica coastline from the IMS receive stations is partly blocked by islands and topographic features of the coast, but the blockage sectors are narrow relative to the observable part of the Antarctic coast.

REFERENCES

- Chapp E., Bohnenstiehl D. R., *et al.* (2005), *Sound-channel Observations of Ice-generated Tremor in the Indian Ocean*, *Geochemistry, Geophysics and Geosystems*, v.6;
- Chiu B. S., Miller J. H., *et al.* (1995), *Forward coupled-mode propagation modeling for coastal acoustic tomography*, *J. Acoust. Soc. Am.*, v.99(2), pp. 793-802;
- Gavrilov A.N. and Mikhalevsky P.N. (2006), Low-frequency acoustic propagation loss in the Arctic Ocean: Results of the Arctic climate observations using underwater sound experiment, *J. Acoust. Soc. Am.*, v.119(6), pp. 3694-3706;
- Gavrilov A.N. and Mikhalevsky P.N. (2001), *Mode-coupling effects in acoustic thermometry of the Arctic Ocean*, in: *Inverse Problems in Underwater Acoustics*, Taroudakis M. and Makrakis G. edited, Springer-Verlag NY, pp. 105-125;
- Gavrilov A.N. and Vazques G. (2005), Detection and localization of ice rifting and calving events in Antarctica using remote hydroacoustic stations, *Proceedings of ACOUSTICS 2005*, Busselton, Western Australia;
- Hanson J.A. and Bowman J.R. (2006), Methods for monitoring hydroacoustic events using direct and reflected T waves in the Indian Ocean, *Journal of Geophysical Research*, v.111 (B02305);
- Menke W., (1984), *Geophysical Data Analysis: Discrete Inverse Theory*, Academic Press, New York;
- Talandier J., Hyvernaud O., *et al.* (2002), Long-range detection of hydroacoustic signals from large icebergs in the Ross Sea, Antarctica" *Earth and Planetary Science Letters*, v.203, pp. 519-534.